A NEW DETAILED MULTI-BODY MODEL OF THE PEDESTRIAN LOWER EXTREMITY: DEVELOPMENT AND PRELIMINARY VALIDATION

Jason Kerrigan, Dan Parent, Costin Untaroiu, Jeff Crandall, Bing Deng*
University of Virginia Center for Applied Biomechanics
***Vehicle Development Research Lab, General Motors R&D Center**

ABSTRACT

The goal of this study was to develop a mathematical model of the lower extremity capable of predicting injury risk and simulating the kinetic and kinematic response of the pedestrian lower extremity under vehicle impact loading. The hip-to-foot multi-body model incorporates a detailed facet contact surface, 50th percentile male anthropometric and inertial properties, and stiffness and failure tolerances from the most recent literature. Model validation was achieved using a combination of parameter optimization for component-level kinetic response and full-scale simulations for kinematic response. The three-dimensional kinematic response of the struck-side lower extremity of seven post-mortem human surrogates struck laterally by a sedan at 40 km/h is also presented.

Keywords: Pedestrians, Multibody, Models, Optimization Methods

VEHICLE SAFETY PROFESSIONALS have been working to develop human body mathematical models to study vehicle-pedestrian impacts in an effort to develop injury risk assessment tools, injury countermeasures and accident reconstruction techniques. The finite element (FE) method, which is commonly used to develop human body mathematical models, provides for the modeling detail necessary to accurately represent detailed geometries, a variety of contact algorithms, complex material constitutive models, and local material response measurements that can be used to predict tissue failure. However, to take full advantage of the benefits provided by the FE method considerable computational power and time are required to perform model simulations. While recent technological advancements have resulted in improved biofidelity and utility of human pedestrian FE models (Snedeker et al. 2003, Arnoux et al. 2005, Untaroiu 2005, Kikuchi et al. 2006), questions still exist regarding whether the increased detail afforded by FE models is justifiable given the currently available computational technology and experimental data. For instance, a recent subject-specific FE modeling study showed that after matching the structural response of a human femur loaded in three-point bending by optimizing the bone material properties, the detailed FE model predicted bone surface strains different from those measured in the tests (Untaroiu et al. 2006). Thus, an FE model that relies on strain-based injury criteria may not accurately predict the time and/or location of injury despite exhibiting an accurate structural response in a component-level simulation.

On the other hand, while not able to represent detailed geometries or material level responses, pedestrian multi-body mathematical models (cf. Ishikawa et al. 1993, Yang et al. 2000, Neale et al. 2003) continue to be used extensively by both manufacturers and researchers to predict and analyze the complex kinetics and kinematics of vehicle-pedestrian impacts (cf. Okamoto et al. 2003, van Rooij et al. 2003, Kuehn et al. 2005, LeGlatin et al. 2006, Yao et al. 2007). Multi-body models sacrifice the ability to predict local responses in exchange for considerable reductions in computational time, permitting their use in iterative vehicle design and accident reconstruction efforts. The most recent, advanced and commonly used multi-body model (van Hoof et al. 2003), which incorporates 52 rigid bodies and a 64 ellipsoid exterior, was developed for use in MADYMO. While the model was developed using the most advanced biomechanics data available at the time, it has several downsides with regard to both its biofidelity and its architecture. Despite evidence that bone exhibits a rate-sensitive response, the response characteristics of the leg and thigh models are based on stiffnesses measured in quasi-static bending tests. The model's knee bending response and injury tolerance are based on a series of biomechanical investigations (Kajzer et al. 1997, 1999) that have been shown to employ an inadvertent calculation error that resulted in overestimation of the knee joint bending stiffness and injury tolerance (Konosu et al. 2005). Additionally, since ellipsoids have been used to

model the exterior, modeling contact with either ellipsoid or facet surfaces can result in computational problems that affect model response kinematics.

Rather than improving the model developed by van Hoof et al. (2003), the goal of the current study was to build an entirely new model that not only incorporates the most advanced biomechanical data available, but also utilizes a more biofidelic geometry, and advances in injury modeling. As an initial step, this study focuses on the development and validation of a lower extremity model due to the frequency of injuries to the lower extremity and the importance of the interaction between the lower extremity and vehicle in subsequent impact dynamics. Pedestrian epidemiological data suggest that the lower extremity is either the most or the second most frequently injured body region (Kong et al. 1996, Edwards and Green, 1999, Peng and Bongard, 1999, Chidester and Isenberg, 2001, Mizuno 2003, Toro et al. 2005). Furthermore, vehicle interaction with the lower extremity has been shown to affect upper body kinematics (Kerrigan et al. 2007), which can affect injury risks by altering head, thoracic and pelvic impact locations and velocities.

The lower extremity model was constructed using 50th percentile male anthropometric and inertial properties, and structural response and injury tolerance properties from the literature. The model incorporated both external and internal anatomical geometry and the ability to model the effects of injury. Leg and thigh model parameters were simultaneously optimized in simulations replicating previously published experiments (Kerrigan et al. 2004, Ivarsson et al. 2004, Ivarsson et al. 2005) until model responses matched scaled response corridor averages. The model leg and thigh were connected via a knee joint, and then connected to existing foot/ankle (Hall et al. 1998) and upper body (van Hoof et al. 2003) models. The model's response to full-scale vehicle impact was verified by comparing its local rotational and global translational kinematics to that of post mortem human surrogates (PMHS) in simulations designed to replicate previous experiments (Kerrigan et al. 2007). In the experiments, the PMHS were instrumented with custom six-degree of freedom instrumentation packages to capture the three dimensional kinematics of the lower extremities, and previously unpublished data from the sensors are included here to assist in evaluating the model's response.

METHODS

MODEL DEVELOPMENT : In the current study, a multi-body model of the 50th percentile male right lower extremity was developed in MADYMO (v. 6.3.2, TASS, Delft, The Netherlands). To determine the structural and injury-predictive capabilities of the model the epidemiology, forensic and injury biomechanics literature were reviewed to determine the most common pedestrian lower extremity injuries and their mechanisms (Kerrigan 2008). In general, the most commonly reported pedestrian lower extremity injuries are diaphyseal fractures of the long bones (tibia, fibula, femur), fractures and soft tissue injuries to the knee joint, and malleolar fractures. Since the majority of pedestrians are struck laterally (Kam et al. 2005), it is easy to see that laterally directed bending and shearing loads to the lower extremity are responsible for the majority of lower extremity injuries in lateral impacts (Yang et al. 2005). Furthermore, both the current study and previous biomechanical studies (cf. Cesari et al. 1980) involving PMHS lower extremities loaded laterally by vehicles or vehicle-like structures have produced bending (wedge) fractures of the diaphyseal long bones, fractures and soft tissue injuries to the knee joint that are the result of bending and shearing loads, and malleolar fractures resulting from severe inversion/eversion loading of the ankle joint. Thus the current model was developed with the ability to simulate both lateral and anterior-posterior (AP) bending along its entire length as well as the ability to predict bending injuries in the thigh and leg, bending and shearing injuries in the knee, and inversion/eversion injuries in the ankle.

Model Architecture : The hip joint was modeled as a spherical joint, possessing three orthogonal rotational degrees of freedom (DOF), based on its anatomical functionality. The leg and thigh were each modeled with three spherical joints, approximately equally spaced along the length of each segment, to simulate bending deformations. To permit both bending and shearing at the knee joint, as well as to allow for axial compliance within the lower extremity, the knee joint was modeled as a free (6 DOF) joint. The detailed ankle and foot multi-body model developed by Hall (Hall 1998, Hall et al. 1998) was incorporated into the model. Hall's model contains a universal joint to model talocrural (tibio-talar) joint rotations in the dorsiflexion/plantarflexion and inversion/eversion directions, a revolute joint to model subtalar joint rotations in the inversion/eversion direction, a spherical joint to model the midtarsal joint, and two revolute joints to model the tarso-metatarsal and metatarso-

phalangeal joints. Each of the eight lower extremity (hip to distal leg) joints was separated by a single discrete mass (7 total), with an additional mass separating the distal leg joint from the ankle model.

Anthropometric and Inertial Properties : The anthropometric and inertial properties of the model (other than those of the foot/ankle model) were derived from the General Motors (GM)/University of Virginia (UVA) 50th percentile male FE model (Untaroiu 2005, Untaroiu et al. 2005). The FE model consists of bones (femur, tibia, fibula, and patella), various soft tissues around the knee joint, the flesh surrounding the long bones, and a skin surface. The geometry of the model's long bones, flesh, and skin were scaled from the normal male geometry of the Visible Human Project developed by The National Institutes of Health's National Library of Medicine (NLM, 1996). The inertial properties of the FE model were derived from implementing individual densities for each of the models materials including cortical bone (2 g/cm^3), trabecular bone (1.1 g/cm^3), flesh (1.0 g/cm^3), and skin (0.8 g/cm^3) (Untaroiu et al. 2005).

The GM/UVA FE lower extremity model was cut into eight (four each for the leg and thigh) section to determine the geometric and inertial properties of the multi-body model (Figure 1A). The thigh and leg sections of the multi-body model were defined as the portions of the FE model between the Hip Joint Center and the Knee Joint Center, and between the Knee Joint Center and the Ankle Joint Center, respectively (Figure 1A). From each of the four leg and four thigh sections, the mesh of the FE model skin was extracted for use as the facet contact surface of the multi-body model. The mass, center of gravity (CG), and diagonal elements of the mass moment of inertia tensor (about the section center of gravity) of each of the eight sections of the FE model were determined (Table 1) by performing custom simulations with the LS-DYNA (ver. 970, LSTC, Livermore CA) non-linear finite element solver. The model local coordinate system was based on the SAE convention for the standing human: +X pointing anterior, +Y pointing to the right, and +Z pointing down (SAE J211, 1995).

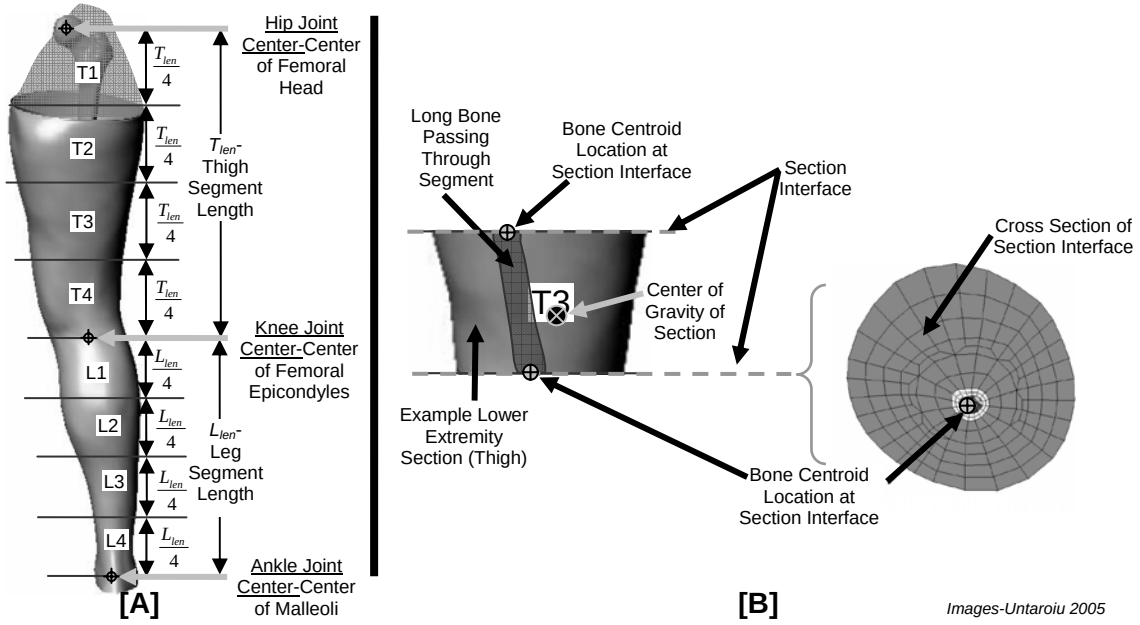

Fig. 1. Schematic Describing How the UVA FE Model Was Cut Into Eight Sections [A], and How Joint Locations and Body Centers of Gravity Were Determined [B].

Table 1. Inertial Properties of the Lower Extremity Model.

Body	Mass (kg)	Moment of Inertia (kgm^2)			CG From Hip Joint Center (mm)		
		Ixx	Iyy	Izz	X	Y	Z
T1	1.643	3.748E-03	4.235E-03	5.719E-03	-1.3	13.2	76.2
T2	2.865	7.556E-03	8.332E-03	1.142E-02	2.6	-5.1	153.7
T3	2.425	5.694E-03	6.495E-03	7.779E-03	9.7	-15.8	250.2
T4	1.746	3.423E-03	3.726E-03	4.066E-03	15.1	-29.0	354.1
L1	1.231	2.207E-03	2.348E-03	2.416E-03	8.0	-21.5	460.4
L2	1.296	2.085E-03	2.268E-03	2.349E-03	-7.0	-14.4	554.4
L3	0.703	8.632E-04	9.270E-04	7.039E-04	-6.1	-14.0	648.0
L4	0.370	4.553E-04	4.763E-04	2.199E-04	-2.5	-19.3	744.0
Total Mass	12.279						

The four bodies in each segment (leg and thigh) were connected with three spherical joints that were located at the interfaces between adjacent sections longitudinally, and at the long bone area centroid transversely (Figure 1B and Figure 2). The hip, knee and ankle were located at their respective Joint Centers (Figure 1A, Figure 2). The joint coordinate systems of the leg joints were oriented so that they were aligned with the model local coordinate system. The joint coordinate systems of the thigh joints were oriented similarly, however each thigh joint was rotated (8.1-12.2 degrees) about the local X-axis until its local Z-axis intersected the next joint distally to account for the anatomical curvature of the femur (Figure 2B).

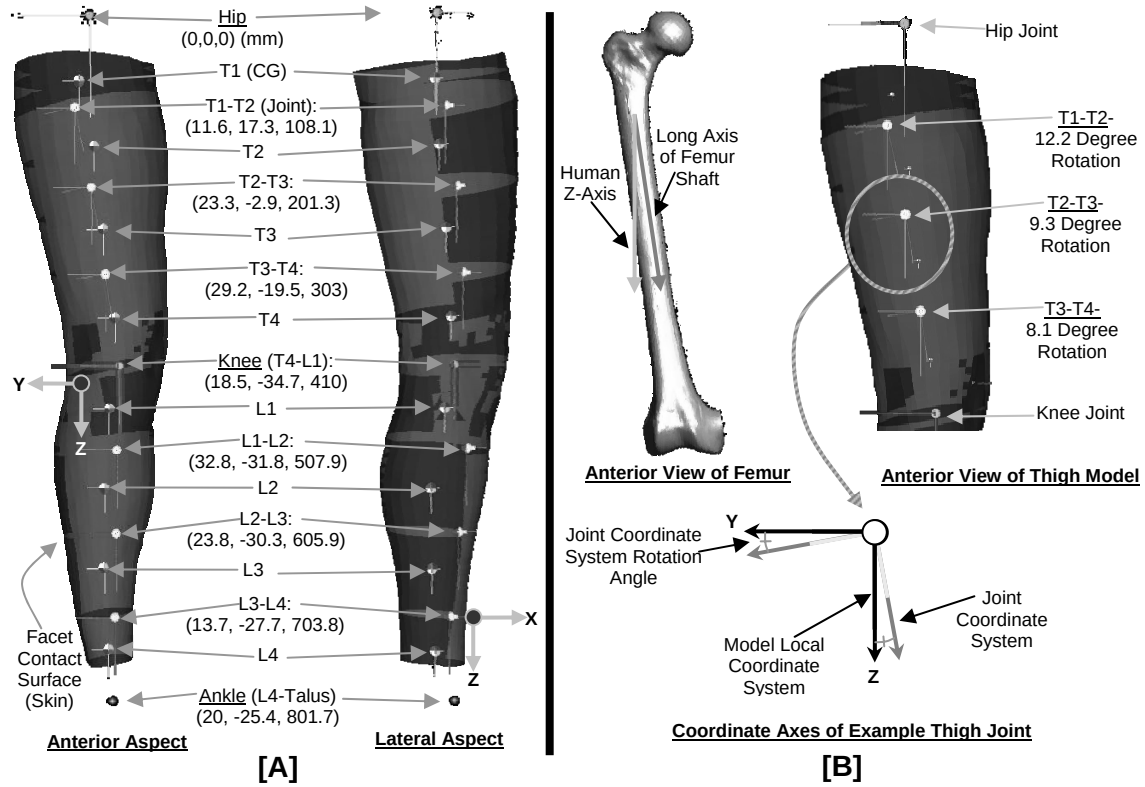

Fig. 2. Lower Extremity Model With Joint Coordinates [A] and Thigh Joint Rotations [B].

Contact Modeling : Each of the four leg and four thigh skin FE meshes was modeled in MADYMO as a facet surface (QUAD4 and MEM4, with "null" material properties) (TNO 2006). To maintain the relationship between the geometric and inertial properties of the FE model, each facet skin model section remained fixed with respect to the CG of its respective mass (Table 1).

Injury Modeling : The body/joint structure of the model was configured to permit the model to simulate the effects of injury to the thigh, knee, and leg. The joints discussed previously, hereafter referred to as "pre-injury joints", modeled the structural deformation of the lower extremity. To facilitate injury modeling, using a method similar to that implemented by van Hoof et al. (2003), additional joints, referred to as a "post-injury joints", were added at the same locations as the pre-injury joints at the knee, mid and distal thigh, and all three leg joints. Pre-injury and post-injury joints were separated by masses (1 g each) to maintain the chain structure of the model. The post-injury joints start in a locked (constrained) configuration, and when an injury occurs at a particular location, the pre-injury joint locks, and the post-injury joint unlocks (removing the constraints). Injury occurrence was determined by comparing moment, force, displacement or angle of the particular joint DOF to a prescribed injury tolerance limit. While all of the pre-injury joints (except the knee) were spherical joints, free joints were used for the post-injury joints to permit release all of the stored energy at the time of injury and to ensure the model could undergo shear deformations after injury.

Structural Response and Injury Tolerance: The structural response of the model was specified via defined point and Cardan restraints that apply resistance to motions between connected bodies. Cardan restraints were used at each of the spherical joints, and a Cardan restraint was used in

conjunction with a point restraint at the knee joint. The Cardan restraints were aligned with the joints (including femoral joint rotations, Figure 2B).

More than 60 studies reporting lower extremity biomechanical response and injury tolerance data from tests on PMHS and volunteers were reviewed (Kerrigan 2008), and the data most applicable to vehicle-pedestrian impact loading were selected for inclusion as nonlinear (multi-point) loading characteristics and injury criteria in the model (Table 2). For the hip the zero degree knee flexion flexion/extension stiffness (Reiner and Edrich 1999) was used and the abduction response (Engin 1979) was reflected to determine the adduction response (which resulted in a response similar to the commonly-referenced stiffness implemented by Yang and Lovsund (1997)). The zero degree knee flexion stiffenss was selected for the flexion/extension (Reiner and Edrich 1999), torsion (Markolf et al. 1976), and AP shear (Markolf et al. 1976) knee characteristics. The tensile stiffness of the knee joint was estimated as the sum of six individual knee ligament stiffnesses tested by van Dommelen et al. (2005) and reported by Kikuchi et al. 2006. The valgus bending corridor average reported by Ivarsson et al. 2004 was reflected to determine the varus bending response. The corridor average reported by Ramet et al. (1995) for PMHS knees loaded in quasi-static lateral-medial (LM) shear was used since it depicted a stiffness similar to that reported for the two dynamic experiments presented by Bhalla et al. (2003). The dorsiflexion/plantarflexion and inversion/eversion stiffnesses used in Hall's (1998) model were originally specified by combining restraints with ellipsoid contact characteristics between the tibia, fibula, and talus. Since the model developed for this study did not include ellipsoid surfaces for the tibia and fibula, new stiffness functions were implemented for talocrural and subtalar restraints using data presented by Funk et al. (2002) and Rudd et al. (2004). The stiffness functions for the foot joints implemented by Hall (1998) were maintained in the current model.

Table 2. Biomechanical Data Sources.

	Mode	Response Data Source	Injury Criteria Source
Hip	**Flexion/ Extension**	Riener and Edrich 1999	N/A
	Abduction/ Adduction	Engin 1979	N/A
	Internal/ External Rotation	Engin 1979	N/A
Thigh	**LM Bending**	Ivarsson 2004, Ivarsson 2005	Kerrigan 2004, Ivarsson 2005
	AP Bending	Ivarsson 2004, Ivarsson 2005	Kerrigan 2004, Ivarsson 2005
	Torsion	Martens 1980	N,A
Knee	**Flexion/ Extension**	Riener and Edrich 1999	N/A
	Torsion	Markolf 1976	N/A
	Varus/Valgus Bending	Ivarsson 2004	Bose 2008
	Tension/ Compression	Dommelen 2005, Hirsch and Sullivan 1965	N/A
	AP Shear	Markolf 1976	N/A
	LM Shear	Ramet 1995 and Bhalla 2003	Bose 2008
Leg	**LM Bending**	Ivarsson 2004, Ivarsson 2005	Kerrigan 2004, Ivarsson 2005
	AP Bending	Ivarsson 2004, Ivarsson 2005	Kerrigan 2004, Ivarsson 2005
	Torsion	Martens 1980	N/A
Ankle	**Dorsiflexion/ Plantarflexion**	Rudd 2004	N/A
	Inversion/ Eversion	Funk 2002	N/A

LEG AND THIGH PARAMETER OPTIMIZATION : The bending moment vs. deflection response corridors presented by Ivarsson et al. (2004 and 2005) could not be implemented directly in the model since moment vs. angle data were required for the leg and thigh Cardan restraints. Thus the nonlinear Cardan restraint loading characteristics, as well as the facet surface contact characteristics, were determined using parameter optimization simulations designed specifically to replicate the experiments discussed by Ivarsson. Simulations were performed for each of the five loading characteristics for which Ivarsson et al. (2004 and 2005) presented corridors.

Experiments : PMHS leg and thigh specimens were cleared of the soft tissues around their epiphyses and potted in rigid potting cups attached to rollers that rested on greased support plates (Figure 3). Specimens were loaded in dynamic (approximately 1.5 m/s) LM three-point bending to failure with a ram attached to the actuator of a material testing machine. Moment time histories were determined from the reaction forces measured in the support load cells and dynamic calculations of the support moment arms. Specimen responses were geometrically scaled to represent the response of a 50^{th} percentile male and single standard deviation moment vs. deflection corridors were developed for each of the five loading conditions (Ivarsson et al. 2004, Ivarsson et al. 2005).

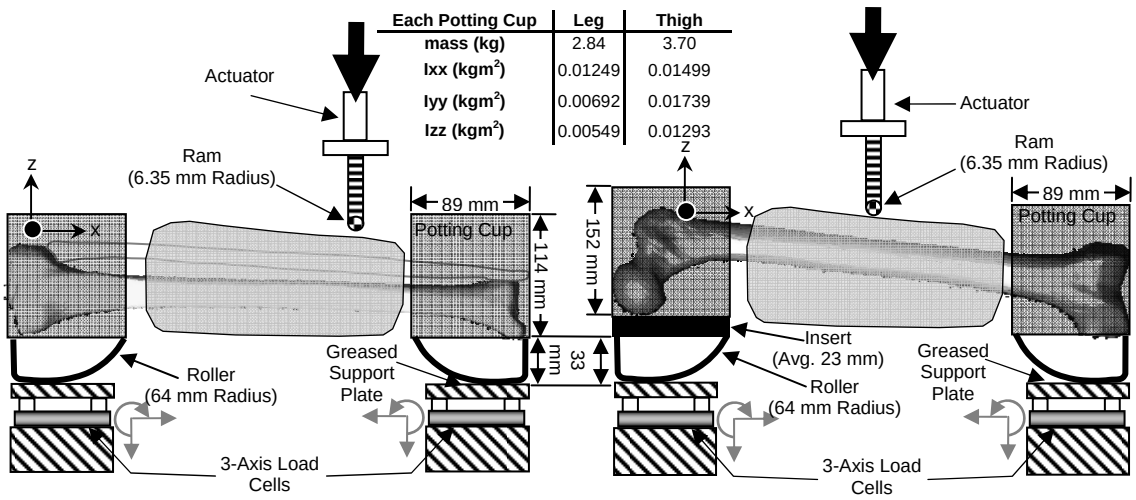

Fig. 3. Distal Third Leg Bending (Left) and Mid Span Thigh Bending (Right) Schematics.

Simulations : Distal third, mid span, and proximal third leg and distal third and mid span thigh bending simulations were set up using identical conditions to those employed in the experiments (Figure 4). The leg and thigh models were fixed to potting cups and rollers with identical geometric and inertial (Figure 3) properties and a low friction contact was employed at the interface between the rollers and supports. Loading was applied using an identical displacement-controlled ram at the same relative locations as in the experiments. Moment time histories were calculated using support reaction forces multiplied by dynamically measured moment arms (as in the experiments).

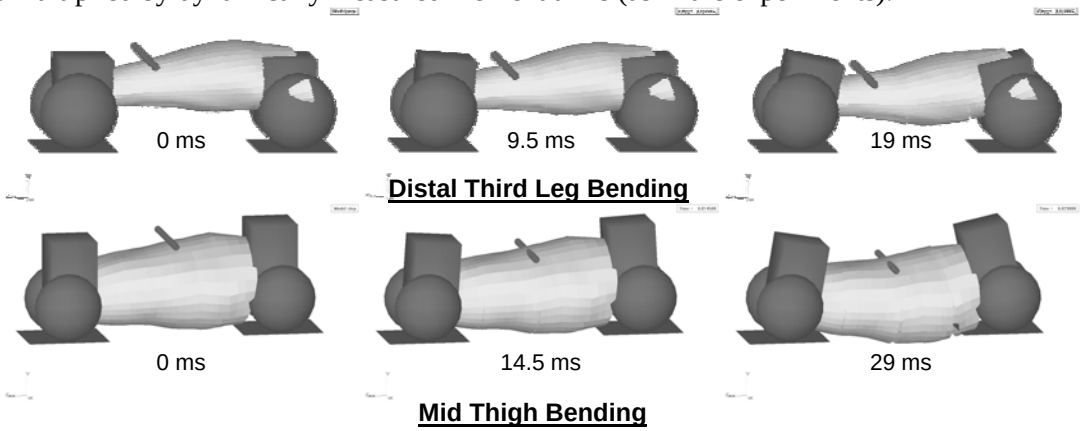

Fig. 4. Distal Third Leg Bending (Top) and Mid Span Thigh Bending (Bottom) Simulations.

Optimization Routines : All optimization routines were performed using the commercially available software package modeFRONTIER (version 3.2.2, ESTECO s.r.l., Trieste, Italy). One optimization routine was used within modeFRONTIER to optimize the structural response of the leg using the three different loading configurations, and one routine was used to optimize the structural response of the thigh using the two different loading configurations. The optimization routines were coupled to a custom MATLAB code that calculated the applied moments and objective functions for each simulation.

Four and five moment-angle data points were used to define the elastic characteristics of the thigh and leg restraints respectively. Damping coefficients were added at each joint to define the portion of the kinetic response responsible for the loading rate sensitivity. Three data points were used to characterize the elastic loading characteristic of each of the leg and thigh facet surfaces. The last data point in each restraint and contact characteristic was not adjusted during the optimization. By examining the corridors presented by Ivarsson et al. (2004 and 2005), it was hypothesized that the PMHS flesh deformed under ram loading with relatively low stiffness until it "bottomed-out" and the stiffness became substantially higher (when bone loading began). Thus the second data point for each contact characteristic was chosen to coincide with the hypothesized "bottoming-out" point on the

average curve of each response corridor. A total of 29 and 23 input variables (including the remaining Cardan loading points, damping coefficients and first point of each contact characteristic) were optimized in the leg and thigh bending optimization routines respectively.

Each of the two (leg and thigh) optimization schemes simultaneously minimized two objective functions. The first objective function measured the difference between the model's segment moment-angle response and the average response defined by the experimental corridors (Ivarsson et al. 2004, Ivarsson et al. 2005). The second objective function was used to restrict the magnitude of the Cardan restraint damping coefficients since the damping torque competed directly with the elastic torque. A second objective function was constructed so that its minimization resulted in a ratio of dynamic (damping plus elastic) to static (elastic) torques of 1.69, since this is the ratio of the dynamic to the static bending strength and stiffness of the human leg presented by Schreiber et al. (1997)

Using an initial range for each variable, modeFRONTIER's Cross Validation exploratory design of experiment method, which utilized the Kriging interpolation method (cf. Kerry and Hawick 1998) to uniformly distribute designs within the design space, was used to select an initial set of simulations. The optimization scheduler used was the Non-dominated Sorting Genetic Algorithm II (NSGA II), which is a fast, elitist, multi-objective evolutionary algorithm (cf. Deb and Goel, 2001). Optimization routines were continued until improvement of the objective functions was only negligible from routine to routine.

Injury Criteria Determination : Using the optimized parameters, one simulation was performed for each of the five cases until the segment moment (normal support force multiplied by dynamically measured moment arm) equaled a 50% risk of fracture as determined from the published injury criteria (Kerrigan et al. 2004, Ivarsson et al. 2005). The moment measured in the Cardan restraint closest to the impact location (i.e. distal restraint for distal bending) at the instant when the segment moment equaled a 50% risk of injury was used as the injury criteria for that joint.

EXPERIMENTAL CHARACTERIZATION OF FULL-SCALE IMPACT KINEMATICS : To verify the full-scale impact kinematic response of the model, the model's response to vehicle impact needed to be compared to the detailed experimental kinematics data. To characterize the full-scale impact kinematic response of the pedestrian lower extremity, previously unpublished data from seven full-scale vehicle-pedestrian impact experiments with PMHS impacted by a mid-sized sedan at 40 km/h (Kerrigan et al. 2007) were used.

Testing : Seven PMHS were selected based on the absence of fractures or other bone pathology and to provide for the greatest variation in their statures (Table 3). The PMHS were obtained and treated in accordance with the ethical guidelines established by NHTSA, and all testing and handling procedures were reviewed and approved by an independent Oversight Committee at UVA.

Table 3. Full scale test specimen information.

PMHS ID	Age/ Gender	Mass (kg)	Stature (cm)	BMI (kg/m^2)	Right Leg Length (mm)	Right Thigh Length (mm)	Sum Length (mm)	Right Leg Angle (deg)	Right Thigh Angle (deg)
S1	67/F	63.5	163.1	23.9	389	341	730	58	84
S2	57/F	88.8	164	33	332	374	706	64	86
S3	71/F	82.5	164.5	30.5	387	379	766	64	85
M4	32/F	90.6	172.9	30.3	355	343	698	61	91
M5	49/F	92.9	174.3	30.6	383	366	749	59	88
T6	70/M	87	179	27.2	415	407	822	57	99
T7	74/M	91.6	184.3	27	444	414	858	66	92
Average	60	85.3	171.7	28.9	386	375	761	62	90
COV	25%	12%	5%	11%	10%	8%	8%	5%	6%

Each specimen was instrumented with four six-degree-of-freedom (6DOF) cubes, one at each distal femur and at each proximal tibia, to facilitate kinematics measurement during the tests. Each 6-DOF cube (or simply "cube") contained three accelerometers (model 7264B-2000, Endevco Corp., San Juan Capistrano, CA) and three magnetohydrodynamic (MHD) angular rate sensors (model ARS-06, Applied Technology Associates, Albuquerque, NM) mounted orthogonally. The six sensors in each cube were arranged in a specially designed aluminum cube to allow measurement of both accelerations and velocities about the cube's three orthogonal axes. The cubes were rigidly fixed to the bones using established methods (Kerrigan et al. 2008).

PMHS specimens were supported in a standing position via a support harness attached to a solenoid release mechanism designed to release each specimen approximately 25 ms prior to vehicle impact. Specimens were positioned in mid-stance gait with their right—struck-side—lower extremity positioned back. After positioning, a coordinate measurement machine (CMM) was used to digitize the orientations of the cubes with respect to the global (inertial) reference frame, and to make measurements of the pre-impact position of each specimen. Specimen anthropometry including the right thigh length and angle (between the greater trochanter and the lateral tibial plateau) and the right leg length and angle (between the lateral tibial plateau and the lateral malleolus) were also measured (Table 3). Specimens were struck by the test vehicle at 40 km/h and vehicle PMHS interaction continued for 250 ms after impact (see Kerrigan et al. 2007 for additional test methodology).

Cube Data Processing : Using established 6 DOF cube data processing techniques (Kerrigan et al. 2008) lower extremity cube data were used to determine varus/valgus knee bending angle time histories and the techniques were extended to calculate femoral and tibial global acceleration and velocity time histories. Data from the angular rate sensors in each cube were used to determine the time history of the local-to-global transformation matrix (with the initial transformation determined from the CMM), which specified the orientation of the cube at each time step. From the time history of the transformation matrix, the locally measured accelerations were expressed in the global reference frame and integrated to determine the global velocities.

FULL-SCALE IMPACT SIMULATION : To verify the lower extremity model's response under full-scale vehicle impact loading, simulations were performed under conditions that replicated those used in the experiments. To facilitate full-scale impact simulations, the lower extremity model was mirrored to create the contralateral (left) limb, and both limbs were attached to the pelvis (and upper body) of the model presented by van Hoof et al. (2003). Then a FE shoe model having the same geometric and inertial properties of the shoes worn by the PMHS in the experiments was developed and attached to the distal surface of the foot (Figure 5B). Sensors were added to the distal thigh and proximal tibia models at locations that replicated the average 6DOF cube mounting locations in the PMHS. To facilitate positioning, markers were added to the model to represent the locations of the right greater trochanter, the most lateral point of the tibial plateau, and the lateral malleolus. The model was positioned (Figure 5A) to mimic the average position of the PMHS (Table 3) used in the experiments.

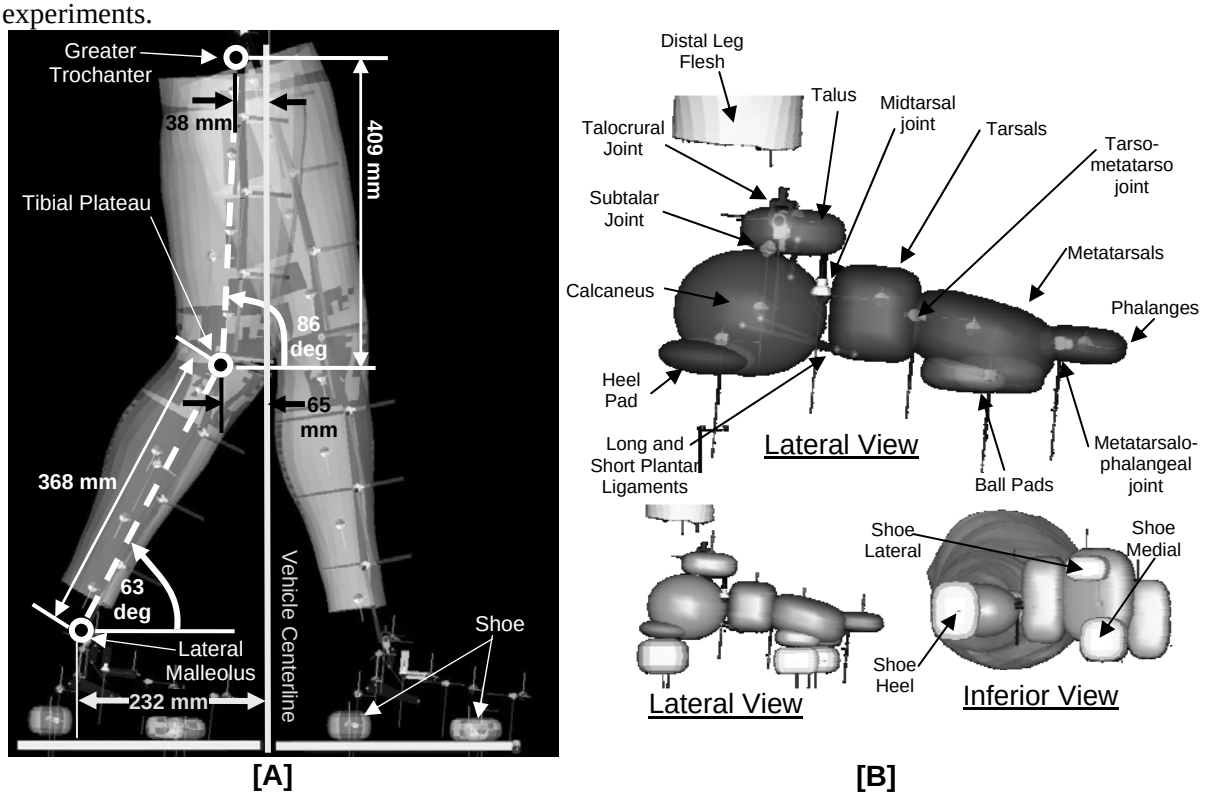

Fig. 5. Pre-Impact Model Position [A] and the Hall (1998) Foot and Ankle Model [B] With (Below) and Without (Above) Shoe.

Vehicle Modeling : Using an FE model of the vehicle that was developed for modeling frontal crash tests, four rigid cylindrical impactor simulations were performed to characterize the contact stiffness of vehicle front end (Figure 6). The locations, sizes, directions and velocities of the impactors were chosen to represent the loading conditions most commonly seen in the experiments (Figure 6). All of the impactors loaded the vehicle 100 mm off the centerline at 40 km/h, and simulations were conducted to allow for 250 mm of deflection to ensure that a more than adequate characterization of the FE vehicle response was performed. By digitizing the front end of the test vehicle with a CMM, a detailed mesh of the test vehicle was developed and implemented in MADYMO as a non-deforming facet surface. Six of the vehicle's front end components were modeled with different contact loading characteristics. An optimization scheme, similar to that described in the Leg and Thigh Parameter Optimization section, was implemented to optimize the nonlinear vehicle contact characteristics of the six vehicle front end components in MADYMO. The objective functions for this optimization scheme were chosen to ensure that the resultant reaction force time history between the MADYMO and FE simulations would match.

Simulation : The full-scale vehicle impact simulation was performed by applying vehicle motion in displacement control at 40 km/h. Gravity was applied to the pedestrian from 0 ms, and the simulation was only performed for 35 ms since the PMHS kinematics data showed that lower extremity accelerations and changes in knee joint bending beyond 35 ms were minimal.

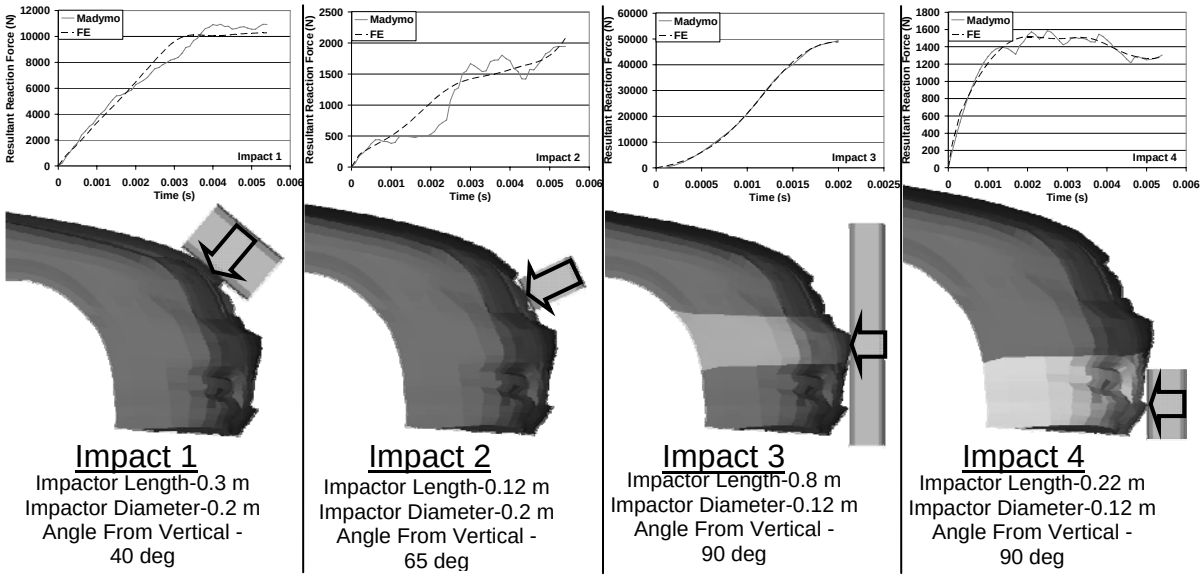

Fig. 6. Vehicle Model Validation Simulations

RESULTS

LEG AND THIGH PARAMTER OPTIMIZATION : All bending simulations were performed using a 1e-5 s time step and the EULER integration algorithm (TNO, 2006) and the absence of a time step effect was verified in simulations performed with a 1e-6 s time step. After optimizing the Cardan restraint loading characteristics, damping coefficients, and skin contact characteristics (Table 4), the leg and thigh bending responses showed excellent correlation with the corridor averages (Figure 7).

Table 4. Optimized Restraint Parameters.

	Skin Contact Characteristics		Proximal Restraint		Mid Restraint		Distal Restraint	
	Penetration (m)	Stress (N/m^2)	Angle (rad)	Moment (Nm)	Angle (rad)	Moment (Nm)	Angle (rad)	Moment (Nm)
Leg	0.0121	25774	0.057	8.9	0.022	15.4	0.057	22.6
			0.109	63.3	0.096	74.5	0.058	108.8
	0.0240	225000	0.278	79.9	0.122	141.6	0.083	166.3
			0.330	153.6	0.185	443.5	0.310	261.4
Thigh	0.0092	26271	0.016	17.7	0.011	22.5	0.013	8.5
	0.0210	227000	0.034	80.0	0.061	120.4	0.048	99.2
			0.068	349.3	0.088	193.3	0.096	162.1
Leg Damping Coefficient (Nms)			2.51		7.48		7.69	
Thigh Damping Coefficient (Nms)			21.19		12.32		10.71	

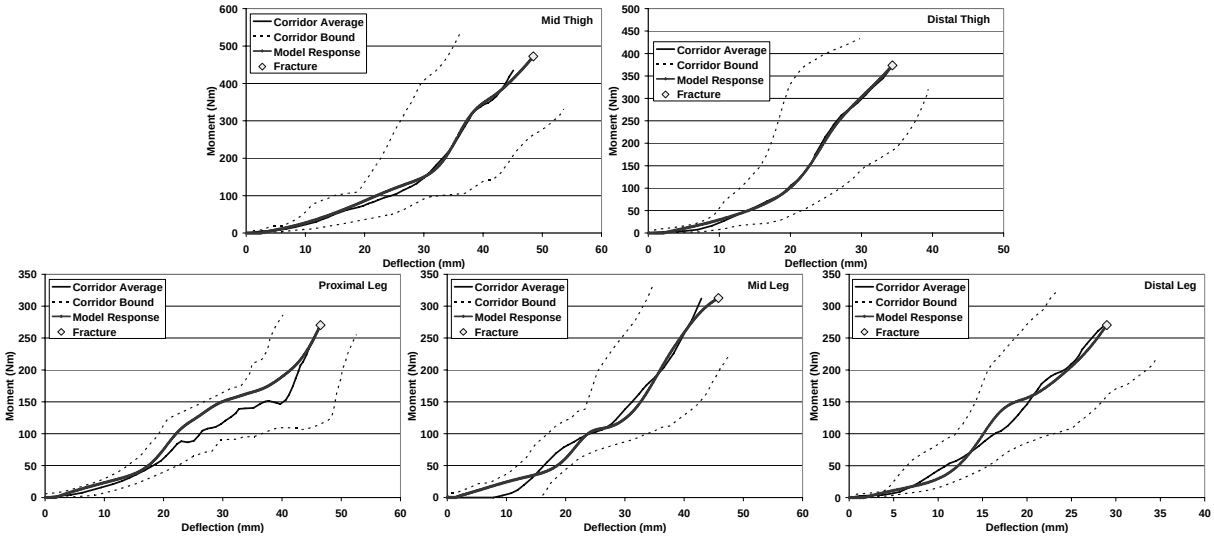

Fig. 7. Model Response with Experimental Corridors.

The last point of each loading characteristic was set higher than the expected loading: 0.6 radians and 5e3 Nm for the restraints, and 0.06 m and 5e8 N/m^2 for the skin. All characteristics passed through the origin. Using the 50^{th} percentile risk of injury (from risk curves in Kerrigan et al. 2004 and Ivarsson et al. 2005), the leg and thigh injury criteria were determined: 492 Nm and 280 Nm for the mid and distal thigh restraints, respectively; 131 Nm, 344 Nm, and 177 Nm for the proximal, mid, and distal leg restraints were respectively.

FULL-SCALE IMPACT EXPERIMENTS AND SIMULATION : The vehicle-lower extremity interaction kinematics of the model (sum of leg and thigh lengths = 777 mm) were compared with those from the S3 experiment (sum of leg and thigh lengths = 766 mm) using posterior view images (Figure 8). In the experiments, four specimens sustained right knee injuries, and three specimens sustained distal third tibia and fibula fractures, with a fourth sustaining an isolated distal third fibula fracture (Table 5). At 5.9 ms and 14.4 ms, the model predicted injuries to the distal leg and knee joint respectively. While two of the experiments resulted in ankle injuries, the model predicted only a 30% risk and 17% risk of injury (Funk et al. 2000) in inversion and eversion, respectively.

While the model knee bending angles, global leg and thigh accelerations, and velocities in all three directions were compared with the PMHS data (Kerrigan 2008), for brevity only the varus/valgus knee bending, the global Z-accelerations, and the global Y-velocities are presented here (Figure 9)

Overall, the model's kinematic response showed good correlation with the PMHS response data. Both the model and the PMHS showed initial valgus knee bending angle rates of approximately 3 deg/ms. The model's knee joint unloads slightly (as a result of the leg injury), but then reloads to knee injury at 14.4 ms. The continued loading (beyond injury) shown in the plot is the result of the post-injury joint deformation. The model predicted that the thigh and leg are initially accelerated upward (107 g) and downward (82 g), respectively, and then downward (54 g) and upward (170 g), respectively. All of the experiments predict a similar downward-then-upward acceleration trend for the leg, however the leg's upward acceleration is nearly double the magnitude of the experiments. For the thigh, experiments S1 and M4 showed similar initial upward accelerations, and all PMHS showed the subsequent downward acceleration with a similar magnitude. While following the same trend as the PMHS, the valgus knee bending angle, leg velocity and acceleration of the model show that the model responds to the vehicle impact slightly (1-2 ms) faster than the PMHS, the thigh velocity and acceleration are more closely aligned with the PMHS data. Additionally, the onset of injury to the knee joint and leg result in abrupt changes in the leg's Y velocity time history without noticeable changes to other signals.

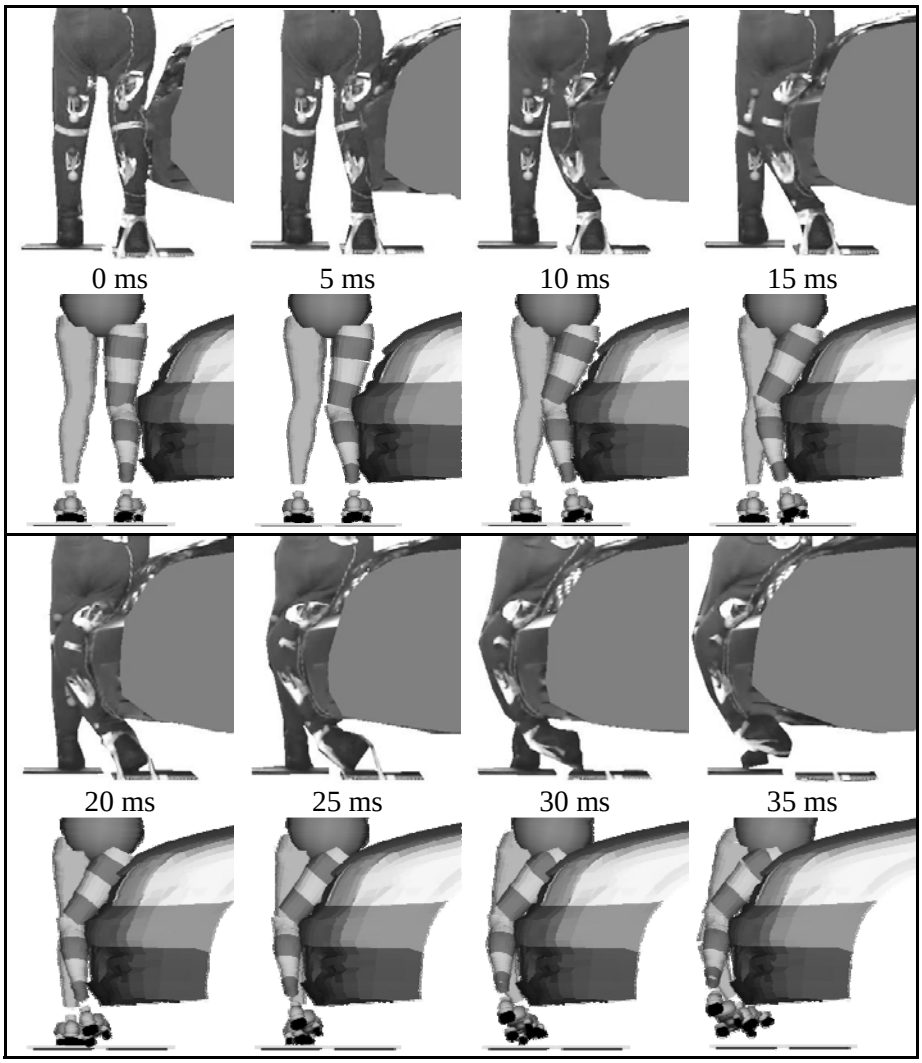

Fig. 8 Model Simulation and Impact Experiment (S3) Kinematics.

Table 5. PMHS Right Lower Extremity Injuries

	Knee	Leg	Other
S1		Distal Third Tibia/Fibula Fracture	
S2	Medial Collateral Ligament (MCL) Laxity	Distal Third Tibia/Fibula Fracture	
S3	Complete Tear MCL, 90% Tear Anterior Cruciate Ligament (ACL)	Distal Third Fibula Fracture	Medial Malleolus Fracture
M4	Complete Tear Medial Collateral Ligament (MCL), Postero-medial corner tear, medial joint capsule tear		
M5	Complete Tear ACL	Distal Third Tibia/Fibula Fracture	
T6	Partial Tear ACL, Medial Femoral Condyle Fracture	Fibular Head Fracture	Tri-Malleolar Fractures, Sub-Trochanteric (Femur) Fracture
T7	MCL Laxity	Fibular Head Fracture	

DISCUSSION

Due to the number of variables (anthropometry, stance, speed, location, geometry, etc.) that can affect pedestrian injury risk, as well as the large range of possible values for each variable, biofidelic, computationally-efficient human body mathematical models validated for vehicle-pedestrian impacts have several applications as both research and design tools.. As research tools, human models can be used to study pedestrian impact kinematics, injury mechanisms, throw distance calculations and in reconstructions studies. As design tools, human models can be used early in the vehicle design process to predict how vehicle structural and styling changes influence pedestrian injury risk. While the FE method has the greatest potential for detailed prediction of injury risk, FE simulations are long (on the order of days in the case of Untaroiu et al. 2005) and computationally-intensive, which restrict

their utility in vehicle design optimization schemes that employ iterative simulations. However, since multi-body models sacrifice modeling deformation and local material response in exchange for considerable reductions in computational time, they provide a more realistic option to optimize vehicle designs. Additionally, in a combined approach, multi-body models could be used to narrow the vast vehicle design space to provide a minimum level of safety for all pedestrians, and FE models could be used for further, detailed refinement. Additionally, a combined multi-body and FE approach can be used to create an efficient tool for use in real-world vehicle-pedestrian impact case reconstructions, similar to the work presented by Ito et al. (2007).

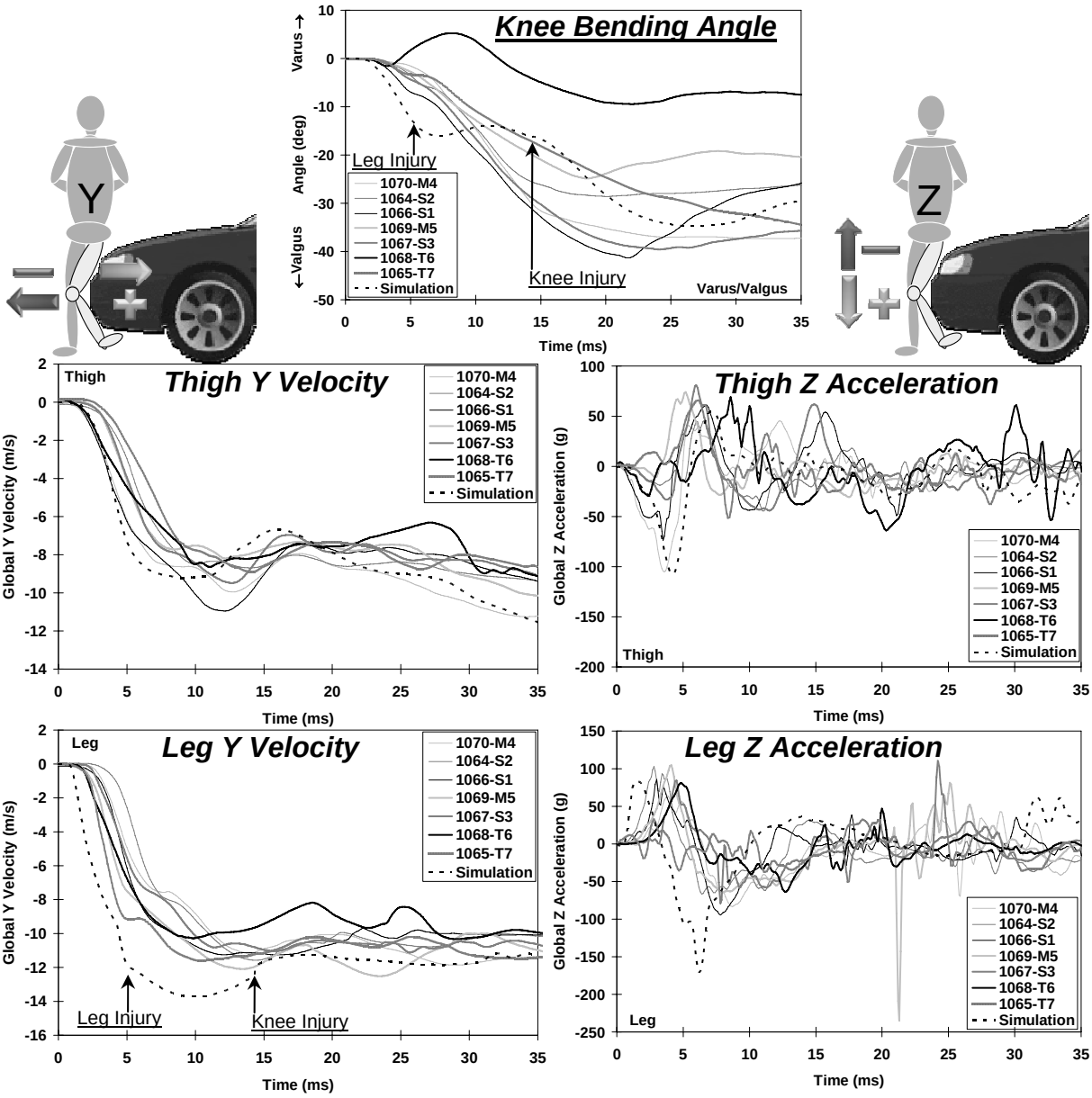

Fig. 9 Lower Extremity Kinematics.

The model presented in the current study maintains the computational efficiency of multi-body models while incorporating advantages over existing multi-body models. Using the model developed in this study, leg and thigh bending simulations required 9 and 12 seconds each, respectively, and full scale simulations required approximately 5 minutes each (2 x 2.2 GHz Intel Xeon processors, 3 GB RAM). Compared to existing models, the current model has several benefits: it incorporates a more realistic geometry, advances in injury modeling, a more detailed representation of the contact surface, and more applicable biomechanics data. The van Hoof et al. (2003) model is compared to the current model in the following sections because it is the most recent, detailed, and extensively validated model

available. It should however be noted that other previous models (Ishikawa et al. 1993, Yang et al. 2000, Neale et al. 2003) suffer from similar and sometimes greater limitations than those of the van Hoof et al. (2003) model discussed below.

To more accurately reflect the geometry and inertial properties of the human lower extremity than the straight (linear) geometry employed by van Hoof et al. (2003), the GM/UVA FE model was used to locate the multi-body model bodies at the actual CG of each model section and the joints at the location of the bone centroid at the interface between model sections. The bone centroid location was chosen as the center of rotation between sections since it is assumed that the bone provides the majority of the stiffness when either the leg or thigh is subjected to bending loading. It should be noted that while it is not clear from van Hoof et al. (2003), it appears that some aspects of the linear geometry were implemented to match the geometry of the Hybrid III dummy.

While able to simulate injuries to the leg and thigh, the model developed by van Hoof et al. (2003) does not release the shear forces when injuries occur at the leg and thigh since post-injury joints are modeled with spherical joints. By using free joints for the post-injury joints, the current model is able to more accurately model how force transmission changes as a result of injury. Additionally, the current model provides the ability to simulate knee joint injuries resulting from either extreme lateral shear displacements or varus/valgus bending angles.

Next, the facet surface used for the model's skin, while not as sophisticated as a fully deformable finite element model, provides for a more realistic representation of the lower extremity's exterior geometry than the ellipsoid-based model utilized by van Hoof et al. (2003). Additionally, since non-physical modeling artifacts can arise when either the pedestrian or vehicle is modeled with ellipsoids, the incorporation of the facet contact surface for the skin results in more realistic contact modeling between the lower extremity and vehicles modeled with finite element or facet surfaces.

Lastly, the model incorporates the most advanced and applicable biomechanics data available to define its response; much of which had not been published when van Hoof's model was developed. New experiments presented by Ivarsson et al. (2004) and Bose et al. (2008) confirmed that the results presented by Kajzer et al. (1997, 1999) incorporated an inadvertent calculation error that resulted in a factor of three or more over-estimation of the knee joint stiffness and failure criteria. The current study also had the benefit of utilizing a detailed structural response and injury tolerance characterization of the leg and thigh under dynamic bending loading presented in Kerrigan et al. (2004), Ivarsson et al. (2004), and Ivarsson et al. (2005).

While the model's response to all five bending tests fell within the corridors, the thigh responses more closely matched the corridor averages than the leg responses (Figure 7) and optimization of the thigh's response occurred in fewer simulations than for the leg (2623 vs. 6804). It is hypothesized that these results are due to a combination of the skewed shape of the leg corridors and because there were only two thigh loading configurations compared to three configurations for the leg. The leg corridors have a skewed shape because Ivarsson et al. (2004) modified the leg response data to account for the substantial reduction in total moment that occurred due the onset of fibula fracture since such a reduction was not permitted in the corridor development technique. The combination of the NSGA II scheduler and the Cross Validation design of experiment provided for faster convergence than other attempted combinations, but thousands of iterations were still required for convergence.

In addition to ensuring that the model's response matched the corridor averages, additional objectives were implemented in the optimizations to balance the contribution of the joint damping with the joint elastic characteristic. In MADYMO, since the total torque applied by a restraint is the sum of the elastic and damping torques, and since the damping torque is a function of the time derivative of the bending angle ($\dot{\varphi}$), damping results in rate-sensitivity to the model. For the leg and thigh bending optimizations, a damping coefficient was used, which resulted in a linear relationship between the damping torque, or the total torque, and $\dot{\varphi}$. However, since the damping coefficients were determined through optimization of the bending test responses, the model's response was only valid at loading rates equal to those used in the bending experiments. Thus, for the full-scale simulation, the linear damping function was changed to a nonlinear function that remained linear up to the peak $\dot{\varphi}$ recorded in the bending simulations, but was exponential beyond peak $\dot{\varphi}$. The exponential relationship, which was based on a characterization of the rate sensitivity of bone from

Carter and Hayes (1977), restricted the restraint damping, and thus the rate-sensitivity of the model, to realistic levels in the full-scale impact simulations (see Kerrigan 2008 for more details).

Since detailed kinematics data were needed for evaluating the performance of the model in full-scale vehicle impacts, unpublished data from previous experiments (Kerrigan et al. 2007) were presented (Figure 9). Since the kinematics and injury data have not previously been presented, a detailed analysis of the observed kinematics and injuries is essential to assist the reader in understanding the details of the kinematics as well as the sources and mechanisms of the injuries. However, since the current study is focused on the development and analysis of a new computational model, discussion of the PMHS kinematics and injuries will be presented in a subsequent study that focuses specifically on the experimental results.

The model's response in the full scale impact simulation showed that the model is capable of replicating the kinematic trends and peak values depicted by the experimental data for 40 km/h lateral impacts with the test vehicle. Additionally, the model predicted the two injuries most common among the PMHS: a distal leg injury and a knee injury. The distal leg injury occurred quite early in the simulation (5.9 ms) and is the result of direct loading by the relatively sharp lower ridge of the test vehicle (Figure 8). The distal leg injury caused brief unloading of the knee joint, but subsequent loading resulted in a bending injury. The only PMHS to sustain both a distal leg injury and a knee injury was S3, which coincidentally was the specimen closest in lower extremity anthropometry to the model. The model's animation showed kinematics similar to those seen in S3 except that the model's leg bounced off the vehicle too early (~25 ms, Figure 8). This is hypothesized to be the result of the relatively coarse mesh of the vehicle in the region of the lower ridge resulting in contact modeling problems at that location. As a next step, the effect of improving the mesh in this region will be evaluated.

While this study focused on a preliminary validation of the model's response to vehicle impact loading, additional (to the vehicle mesh) evaluations aimed at further validation and explorations are planned. Firstly, using the MADYSCALE tool available with the MADYMO software, the model can be scaled to match the specific anthropometries of the PMHS specimens, and subject-specific validation simulations can be performed. To scale the model in this way, user-defined scale factors would be specified, and the MADYSCALE tool would be used to simply multiply scalable model parameters by the appropriate scale factors (identified with scaling tags), and output a scaled model. Next, the model's response can be validated in impacts with different vehicles since detailed PMHS kinematic response data are already available (Untaroiu et al. 2007 and Kerrigan et al. 2008). If data from experiments conducted at other velocities and with surrogates in different stances becomes available, those data could also be used to examine the model's validity under different impact conditions. Additionally, since it has been hypothesized that the active musculature in living human knee joints provides for an increase in stiffness over that of PMHS knee joints, the model could be used to examine the sensitivity of the knee joint stiffness to kinematic and kinetic response. Lastly, Bose et al. (2008) showed that the knee joint has a coupled injury tolerance in shear and bending, which currently cannot be directly implemented in MADYMO using the injury simulation techniques implemented in the current model. However, new techniques are currently being explored for future efforts.

CONCLUSIONS

The goal of this study was to develop and preliminarily validate a new biofidelic, multi-body model of the 50th percentile male pedestrian lower extremity capable of both predicting and simulating the injuries most common when pedestrians are struck by vehicles. The use of a facet surface model of the lower extremity skin and simultaneous optimization of the model's structural response and contact parameters resulted in a model capable of predicting the detailed kinematic response of the lower extremity under mid-sized sedan impact loading at 40 km/h. The model incorporates several advantages over previous models including the a more biofidelic internal and external structure, advances in injury modeling, and use of the most recent and detailed biomechanical response data available. Despite these advancements, the response of the current model has only been compared to PMHS impact response data for a single vehicle, impacting at a single velocity, with the impact surrogates positioned in a single orientation, and as a result further validation is needed prior to extensive application of the model. Lastly, the detailed three-dimensional PMHS lower extremity

kinematics data presented in this study are the most detailed vehicle-pedestrian impact response data available.

REFERENCES

Arnoux P, Cesari D, Behr M, Thollon L, Brunet C. Pedestrian lower limb injury criteria evaluation: a finite element approach. Traffic Injury Prevention, 6:288-297, 2005.

Bhalla K, Bose D, Madeley NJ, Kerrigan J, Crandall J. (2003) Evaluation of response of mechanical knee joint impactors in bending and shear loading. NHTSA, Paper 429, Proc. of the 18th International Technical Conference on ESV, Nagoya, Japan.

Bose D, Bhalla K, Untaroiu C, Ivarsson BJ, Crandall J, Hurwitz S. (2008) Injury tolerance and moment response of the knee joint to combined valgus bending and shear loading. J. Biomechanical Engineering/ASME Transactions, 130(3): 031008.

Carter DR, Hayes WC. (1977) The compressive behavior of bone as a two-phase porous structure. Journal of Bone and Joint Surgery, 4(7): 954-962, 1977.

Cesari D, Ramet M, Cavallero C, Billault P, Gambarelli J, Guerinel G, Farisse J, Seriat-Gautier B, Bourret P. (1980) Experimental study of pedestrian kinematics and injuries. Proc. 1980 International Conference on the Biomechanics of Impacts (IRCOBI), Birmingham, United Kingdom; pp 273-285.

Chidester, A., Isenberg, R., Final report-the pedestrian crash data study. NHTSA Paper 01-248, Proc. 17th Conference on the ESV, Amsterdam, The Netherlands, 2001.

Deb K, Goel T. (2000) Controlled elitist non-dominated sorting genetic algorithms for better convergence. KanGAL Report No. 200004. http://www.iitk.ac.in/kangal. (accessed October 4, 2007).

Dommelen J van, Ivarsson B, Jolandan M, Millington S, Raut M, Kerrigan J, Crandall J, Diduch D. (2005) Characterization of the rate-dependent mechanical properties and failure of human knee ligaments. SAE Transactions, Journal of Passenger Cars–Mechanical Systems, 114(6): 80–90.

Edwards KJ and Green JF. (1999) Analysis of the Inter-Relationships of Pedestrian Leg and Pelvis Injuries. Proc. IRCOBI Conference on the Biomechanics of Impacts, pp. 355-369.

Engin A. (1979) Measurement of Resistive Torques in Major Human Joints. Aerospace Medical Research Laboratory Report AMRL-TR-79-4. April 1979. Downloaded May 29, 2007, http://stinet.dtic.mil/cgi-bin/GetTRDoc?AD=ADA071170&Location=U2&doc=GetTRDoc.pdf.

Funk J, Srinivasan S, Crandall J, Khaewpong N, Eppinger R, Jaffredo A, Potier P, Petit. (2002) The effects of axial preload and dorsiflexion on the tolerance of the ankle/subtalar joint to dynamic inversion and eversion. Stapp Car Crash Journal, 46: 245-265.

Hall G. (1998) Biomechanical characterization and multibody modeling of the human lower extremity. PhD. Dissertation. University of Virginia. Charlottesville, VA.

Hall G, Crandall J, Pilkey W, Thunnissen J. (1998) Development of a dynamic multibody model to analyze human lower extremity impact response and injury. Proc. 1998 International IRCOBI Conference on the Biomechanics of Impact, Bron, France; pp 117-134.

Hirsch G, Sullivan L. (1965) Experimental knee-joint fractures a preliminary report. Acta Orthop. Scandinav., 36: 391-399.

Hoof J van, Lange R de, Wismans J. (2003) Improving Pedestrian Safety Using Numerical Human Models. Stapp Car Crash Journal. 47: 401-436 (SAE-2003-22-0018).

Ishikawa, H., Kajzer, J., Schroeder, G. (1993) Computer Simulation of Impact Response of the Human Body in Car-Pedestrian Accidents. Proc. 37th Stapp Car Crash Conference. SAE Paper No.933129.

Ito O, Okamoto M, Takahashi Y, Mori F, Meissner M, Untaroiu C, Crandall J. 2007. Validation of a human FE lower limb model for a child pedestrian against accident data. Proc. International IRCOBI Conference on the Biomechanics of Injury. Maastricht, The Netherlands: 367-370.

Ivarsson J, Lessley D, Kerrigan J, Bhalla K, Bose D, Crandall J, Kent R. (2004) Dynamic Response Corridors and Injury Thresholds of the Pedestrian Lower Extremities. Proc. 2004 International Conference on the Biomechanics of Impacts (IRCOBI), Graz, Austria.

Ivarsson J, Kerrigan J, Lessley D, Drinkwater C, Kam C, Murphy D, Crandall J, Kent R. (2005) Dynamic Response Corridors of the Human Thigh and Leg in Non-Midpoint Three-Point Bending. SAE Transactions, Journal of Passenger Cars–Mechanical Systems, 114(6): 193-204.

Kajzer, J., Schroeder, G., Ishikawa, H., Matsui, Y., Bosch, U., "Shearing and Bending Effects at the Knee Joint at High Speed Lateral Loading," Society of Automotive Engineers, SAE Paper 973326, 1997.

Kajzer, J., Ishikawa, H., Matsui, Y., Schroeder, G., Bosch, U., "Shearing and Bending Effects at the Knee Joint at Low Speed Lateral Loading," Society of Automotive Engineers, SAE Paper 1999-01-0712, 1999.

Kam C, Kerrigan J, Meissner M, Drinkwater C, Murphy D, Bolton J, Arregui C, Kendall R, Ivarsson J, Crandall J, Deng B, Wang JT, Kerkeling C, Hahn W. (2005) Design of a full-scale impact system for analysis of vehicle pedestrian collisions. SAE Transactions, Journal of Passenger Cars–Mechanical Systems, 114(6): 2268-2282.

Kerry K, Hawick K. 1998. Kriging interpolation on high-performance computers. Lecture Notes in Computer Science 1401: 429-438. Springer Berlin/Heidelberg.

Kerrigan J, Drinkwater DC, Kam C, Murphy D, Ivarsson BJ, Crandall J, Patrie J. (2004) Tolerance of the human leg and thigh in dynamic latero-medial bending. International Journal of Crashworthiness, 9(6): 607–623.

Kerrigan J, Crandall J, Deng B. (2007) Pedestrian kinematic response to mid-sized vehicle impact. Int. J. Vehicle Safety, 2(3): 221-240.

Kerrigan J. (2008) A computationally-efficient mathematical model of the pedestrian lower extremity. PhD. Dissertation. University of Virginia. Charlottesville, VA.

Kerrigan J, Rudd R, Subit D, Untaroiu C, Crandall J. (2008) Pedestrian lower extremity response and injury: a small sedan vs. a large sport utility vehicle. SAE-2008-01-1245, Society of Automotive Engineers, Warrendale, PA.
Kikuchi Y, Takahashi Y, Mori F. (2006) Development of a finite element model for a pedestrian pelvis and lower limb. Paper number 2006-01-0683. Society of Automotive Engineers, Warrendale, PA.
Kong, L. B., Lekawa, M., Navarro, R. A., McGrath, J., Cohen, M., Margulies, D. R., and Hiatt, J. R. (1996). Pedestrian-motor vehicle trauma: an analysis of injury profiles by age. American College of Surgeons Journal 182(1):17-23.
Konosu A, Issiki T, Tanahashi M. Development of a biofidelic flexible pedestrian leg-form impactor (Flex-PLI 2004) and evaluation of its biofidelity at the component level and at the assembly level. Society of Automotive Engineers, SAE paper 2005-01-1879, Warrendale, PA.
Kuehn M, Froeming R, Schindler V. 2005. An advanced testing procedure for pedestrian-car collisions. International Journal of Vehicle Safety, 1(1/2/3): 85-99.
LeGlatin N, Blundell M, Blount G. 2006. The simulation of pedestrian impact with a combined multi-body finite elements system model. Journal of Engineering Design, 17(5): 463-477.
Markolf K, Mensch J, Amstutz H. (1976) Stiffness and Laxity of the Knee--The Contributions of the Supporting Structures. J. Bone and Joint Surgery, 58A(5): 583-594.
Martens M, Audekercke R van, Meester P de, Mulier JC. (1980) The mechanical characteristics of the long bones of the lower extremity in torsional loading. J. Biomechanics, 13:667-676.
Mizuno, Y. (2003). Summary of IHRA pedestrian safety WG activities (2003) proposed test methods to evaluate pedestrian protection afforded by passenger cars, NHTSA Paper 580, Proc. Of the 18th International Technical Conference on Enhanced Safety of Vehicles, Nagoya, Japan.
National Library of Medicine (NLM), The. (1996) The Visible Human Project. National Institutes of Health. http://www.nlm.nih.gov/research/visible/visible_human.html.
Neale M., Hardy B., Lawrence G. (2003) Development and review of the IHRA (JARI) and TNO pedestrian models. Proc. 18th International Conference on the Enhanced Safety of Vehicles (ESV).
Okamoto Y, Sugimoto T, Enomoto K, Kikuchi J. (2003) Pedestrian head impact conditions depending on the vehicle front shape and its construction – full model simulation. Traffic Injury Prevention, 4(1): 74-82.
Peng, R. Y. and Bongard, F. S. (1999). Pedestrian versus motor vehicle accidents: an analysis of 5,000 patients. Journal of the American College of Surgeons 189(4): 343-348.
Ramet M, Bouquet R, Bermond F, Caire Y. (1995) Shearing and bending human knee joint tests in quasi-static lateral load. Proc. 1995 International IRCOBI Conference on the Biomechanics of Impacts. Brunnen, Switzerland.
Riener R, Edrich T. (1999) Identification of passive elastic joint moments in the lower extremities. J. Biomechanics, 32: 539-544.
Rooij L van, Bhalla K, Meissner M, Ivarsson J, Crandall J, Longhitano D, Takahashi Y, Dokko Y, Kikuchi Y. 2003. Pedestrian crash reconstruction using mulit-body modeling with geometrically detailed, validated vehicle models and advanced pedestrian injury criteria. Paper 468. Proc. of the 18th International Technical Conference on the Enhanced Safety of Vehicles (ESV). Nagoya, Japan.
Rudd, R, Crandall J, Millington S, Hurwitz S. (2004) Injury tolerance and response of the ankle joint in dynamic dorsiflexion. Stapp Car Crash Journal, 48:1-26.
Schreiber P, Crandall J, Micek T, Hurwitz S, Nusholtz G. (1997) Static and dynamic bending strength of the leg. Proceedings of the International Conference on the Biomechanics of Impacts (IRCOBI), Hanover, Germany, September 24-26, 1997.
Snedeker J, Muser M, Walz F. Assessment of pelvis and upper leg injury risk in car-pedestrian collisions: comparison of accident statistics, impactor tests, and a human body finite element model. Stapp Car Crash Journal, Vol. 47 (October 2003), pp. 437-457.
TNO. (2006) MADYMO theory manual; release 6.3.2; December 2006.
Toro K, Hubay M, Sotonyi P, Keller E. (2005) Fatal traffic injuries among pedestrians, bicyclists and motor vehicle occupants. Forensic Science International, 2005; 151: 151-156.
Untaroiu C, Darvish, K, Crandall J, Deng B, Wang JT. (2005) A finite element model for the lower limb for simulating pedestrian impacts. Stapp Car Crash Journal, 49: 157-181 (2005-22-0008).
Untaroiu C. (2005) Development and validation of a finite element model of human lower limb. PhD. Dissertation. University of Virginia. Charlottesville, VA.
Untaroiu C, Kerrigan J, Crandall J. (2006) Material identification using successive response methodology with application to a human femur subjected to three point bending loading. Paper Number 2006-01-0063. Society of Automotive Engineers, Warrendale, PA.
Yang J, Lovsund P. (1997) Development and validation of a human-body mathematical model for simulation of car-pedestrian collisions. Proc. 1997 IRCOBI Conference on the Biomechanics of Impacts, Hanover, Germany.
Yang J.K., Lövsund, P., J., Cavallero C., Bonnoit J. (2000) A Human-Body 3D Mathematical Model for Simulation of Car-Pedestrian Impacts. International Journal of Crash Prevention and Injury Control, Vol. 2(2), p. 131-149.
Yang J. (2005) Review of injury biomechanics in car-pedestrian collisions. Int. J. Vehicle Safety, 1(1/2/3): 100-117.
Yao J, Yang J, Otte D. 2007. Head injuries in child pedestrian accidents—in-depth case analysis and reconstructions. Traffic Injury Prevention, 8(1): 94-100.